Journal of Biomedical Optics

SPIEDigitalLibrary.org/jbo

Localized surface plasmon resonance based nanobiosensor for biomarker detection of invasive cancer cells

Yoochan Hong
Minhee Ku
Eugene Lee
Jin-Suck Suh
Yong-Min Huh
Dae Sung Yoon
Jaemoon Yang

SPIE

Localized surface plasmon resonance based nanobiosensor for biomarker detection of invasive cancer cells

Yoochan Hong,[a] Minhee Ku,[b,c] Eugene Lee,[b,d] Jin-Suck Suh,[b,e,f] Yong-Min Huh,[b,e,f] Dae Sung Yoon,[a] and Jaemoon Yang[b,f,g]
[a]Yonsei University, Department of Biomedical Engineering, Maeji 234, Heungup, Wonju, Gangwondo 220-710, Republic of Korea
[b]Yonsei University, College of Medicine, Department of Radiology, Shinchon, Seodaemoon, Seoul 120-752, Republic of Korea
[c]Yonsei University, College of Medicine, Brain Korea 21 Project for Medical Science, Shinchon, Seodaemoon, Seoul 120-752, Republic of Korea
[d]Yonsei University, Nanomedical National Core Research Center, Shinchon, Seodaemoon, Seoul 120-752, Republic of Korea
[e]YUHS-KRIBB Medical Convergence Research Institute, Shinchon, Seodaemoon, Seoul 120-749, Republic of Korea
[f]Severance Biomedical Science Institute (SBSI), Shinchon, Seodaemoon, Seoul 120-752, Republic of Korea
[g]Yonsei University Health System, Severance Integrative Research Institute for Cerebral & Cardiovascular Diseases, Shinchon, Seodaemoon, Seoul 120-752, Republic of Korea

Abstract. In this study, we describe the development of a cancer biomarker-sensitive nanobiosensor based on localized surface plasmon resonance that enables recognition for proteolytic activity of membrane type 1 matrix metalloproteinase (MT1-MMP) anchored on invasive cancer cells. First of all, we prepared biomarker-detectable substrate based on gold nanorods (GNRs) using nanoparticle adsorption method. The sensitivity of the sensing chip was confirmed using various solvents that have different refractive indexes. Subsequently, MT1-MMP–specific cleavable peptide was conjugated onto the surface of GNRs, and molecular sensing about proteolytic activity was conducted using MT1-MMP and cell lysates. Collectively, we developed a biomarker detectable sensor, which allows for the effective detection of proteolytic activity about MT1-MMP extracted from invasive cancer cells. [DOI: 10.1117/1.JBO.19.5.051202]

Keywords: LSPR; cancer; nanobiosensor; molecular sensing; MT1-MMP; biomarker; nanoparticle; enzyme.

Paper 130322SSPR received May 7, 2013; revised manuscript received Jul. 12, 2013; accepted for publication Aug. 20, 2013; published online Dec. 2, 2013.

1 Introduction

1.1 *Localized Surface Plasmon Resonance*

Localized surface plasmon resonance (LSPR) is induced by incident light when it interacts with noble metal nanoparticles that have smaller size than the wavelength of the incident light.[1] When the nanoparticles interact with a light beam, parts of the incident photons are absorbed and the other parts are scattered through nanoparticles. Both absorbed and scattered photons are greatly enhanced when LSPR signals are excited.[2] Consequently, optical spectroscopy is the simplest method to detect LSPR signal on ensemble of the nanoparticles and is generally based on extinction measurements. LSPR signals induced by extinction were obtained using a large amount of nanostructures, such as nanoparticles. The resonance conditions are extremely sensitive to the local dielectric environments of the nanostructures. A shift of the maximum extinction wavelength can be caused by small changes in the refractive index (RI) that is close to the nanostructures.[3] The extremely intense and highly confined electromagnetic fields induced by LSPR exhibit very sensitive sensing probes to detect small changes in the dielectric environments around the nanostructures, which is particularly attractive for biomarker sensing applications.

1.2 *Membrane Type 1 Matrix Metalloproteinase*

The matrix metalloproteinases (MMPs) are a family of zinc-mediated proteinases, and they play an important role in invasion of cancer cells.[4] More precisely, they play a crucial role in degradation of extracellular matrix and remodeling of tissue in the processes of inflammatory regulations and metastatic diseases.[5] In particular, membrane type-1 matrix metalloproteinases (MT1-MMPs) have been researched recently because they have functional roles in proliferation and metastasis of cancer cells.[6–10] In that research, cancerous cells exhibited overexpressed and intensively activated MT1-MMPs on their surfaces and the expression level and proteolytic activity of MT1-MMPs were indicators of cancer invasion.

1.3 *Biomarker Detection Using LSPR*

In recent years, there have been vast efforts to detect biomolecules based on LSPR biosensors.[11–15] The analysis and quantification of biomolecules have demonstrated great potential for precise diagnosis and prognosis and understanding of biomedical processes. The demands for early and precise detection of biomolecules are encouraging evolution of the nanobiosensor field. LSPR sensor is one of the most powerful techniques for ultrasensitive, real-time, and multiplex sensing. Herein, we develop a nanobiosensor based on LSPR for molecular sensing about proteolytic activity of MT1-MMP. The sensitivity of the LSPR sensor was confirmed using various dielectric media and shift of maximum wavelength of LSPR signal for each dielectric medium. We also determined sensitivity of the LSPR sensor through the linear relationship between RI of dielectric media and the maximum wavelength (λ_{max}) of LSPR signal. Subsequently, we conducted molecular sensing of MT1-MMP using conjugation of MT1-MMP–specific

Address all correspondence to: Jaemoon Yang, Yonsei University, College of Medicine, Department of Radiology, Shinchon, Seodaemoon, Seoul 120-752, Republic of Korea. Tel: 82-2-2228-0376; Fax: 82-2-2227-7741; E-mail: 177hum@yuhs.ac

0091-3286/2014/$25.00

targetable and cleavable peptide. We also investigated proteolytic activity of MT1-MMP of invasive cancer cells.

2 Theoretical Model

2.1 *Gans Theory*

In this study, we used a sample substrate composed of gold nanorods (GNRs), and so we explain about a theory that describes the RI changes on nonspherical nanoparticles. The shape of nanoparticles is one of the important factors to detect the LSPR signal. For the nonspherical nanoparticles, extended Mie theory, i.e., Gans theory, is applicable. This theory provides the scattering characteristics for both oblate and prolate spheroidal nanoparticles,[16,17] describing the absorption cross-section for prolate spheroid as

$$\sigma_{\text{abs}} = \frac{\omega}{3c}\varepsilon_m^{3/2} V \sum_j \frac{(1/P_j^2)\varepsilon_2}{[\varepsilon_1 + \{(1-P_j)/P_j\}\varepsilon_m]^2 + \varepsilon_2^2}, \quad (1)$$

where ω is the angular frequency of the extinction radiation, ε_m is the dielectric function of the medium surrounding the metal nanoparticles, and ε_1 and ε_2 are the real and imaginary parts of the dielectric function of the metal nanoparticles, respectively. Furthermore, j represents the three dimensions of the particle and P_j includes P_A, P_B, and P_C, termed depolarization factors, for each axis of the prolate spheroid particle. The depolarization factors anisotropically alter the values of ε_1 and ε_2, and the resulting LSPR peak frequencies are represented as

$$P_A = \frac{1-e^2}{e^2}\left[\frac{1}{2e}\ln\left(\frac{1+e}{1-e}\right) - 1\right],$$
$$P_B = P_C = \frac{1-P_A}{2}, \quad (2)$$

where e is the following factor, including the aspect ratio R of the particle[18,19]

$$e = \left[1 - \left(\frac{B}{A}\right)^2\right]^{1/2} = \left(1 - \frac{1}{R^2}\right)^{1/2}. \quad (3)$$

There are two peaks that result from Eq. (1): one peak corresponds to the transverse plasmon peak and the other to the longitudinal plasmon peak. Moreover, Eq. (1) also provides an intuitive understanding of the effect of aspect ratio on LSPR peak wavelength. Factor ε_m, which is 2 for spherical particles, is $[(1-P_j)/P_j]$, a quantity that increases with aspect ratio and can be much larger than 2. This leads to a red shift of the plasmon peak with increasing aspect ratio.

2.2 *Drude Model*

In general, LSPR sensors fundamentally detect spectral shifts by changes in RI around nanoparticles in surrounding dielectric media.[20] This phenomenon can be explain by the Drude model, represented as

$$\varepsilon_1 = 1 - \frac{\omega_p^2}{\omega^2 + \gamma^2}, \quad (4)$$

where ω_p is the plasmon frequency and γ is the damping factor of bulk metal. On the visible and near-infrared regions, i.e., in the case of $\gamma \ll \omega_p$, Eq. (4) is simplified to

$$\varepsilon_1 = 1 - \frac{\omega_p^2}{\omega^2}. \quad (5)$$

Under the resonance conditions ($\varepsilon_1 = -2\varepsilon_m$),

$$\omega_{\max} = \frac{\omega_p}{\sqrt{2\varepsilon_m + 1}}, \quad (6)$$

where $\omega_{\max}$ is the frequency of LSPR peak. Substituting frequency with wavelength using $\lambda = 2\pi c/\omega$ and then dielectric constant with RI via $\varepsilon_m = n^2$, then Eq. (6) becomes

$$\lambda_{\max} = \lambda_p\sqrt{2n_m^2 + 1}, \quad (7)$$

where $\lambda_{\max}$ is the wavelength at LSPR peak, λ_p is the wavelength corresponding to the plasma frequency of the bulk metal, and n_m is RI of dielectric media. Thus, we can find a linear relationship between wavelength of LSPR peak and RI of surrounding dielectric media.

3 Materials and Methods

3.1 *Preparation of PEGylated Gold Nanorods*

Monodispersed GNRs were synthesized using a seed-mediated growth method as in a previously published protocol.[21] In brief, to prepare the gold-seed solution, 250 μL of $HAuCl_4 \cdot 3H_2O$ (10 mM) solution was added to 7.5 mL of hexadecyltrimethylammonium (CTAB) (93 mM) solution, and then 600 μL of ice-cold sodium borohydride (10 mM) was added to the mixture with vigorous stirring. The mixture was allowed to react for 2 min and stored at room temperature for 4 h, and then a growth solution was prepared as follows. The CTAB solution was prepared under vigorous stirring, and then 80 μL of silver nitrate (10 mM) solution, 50 μL of $HAuCl_4 \cdot 3H_2O$ (10 mM) solution, 55 μL of ascorbic acid (100 mM) solution, and 12 μL of gold-seed solution were successively dropped into prepared CTAB solution and stirred for 30 s. The product solution was stored at room temperature for 24 h. The resultant solution was centrifuged three times at 15,000 rpm for 30 min to remove the excess CTAB molecules and redispersed in 5 mL of deionized water (DW). Polyethylene glycol (PEG)-coated gold nanorods (PGNRs) were synthesized according to our previous report.[22] To prepare PGNRs, GNRs were coated with hetero-bifunctionalized PEG (CM-PEG-SH) as a stabilizer. CM-PEG-SH (50 mg) was added to 5 mL of GNR solution (4.73 mM) and stirred for 48 h at room temperature. The mixture was centrifuged at 15,000 rpm for 30 min to remove unbound CM-PEG-SH molecules and resuspended in 5 mL of DW.

3.2 *Fabrication of LSPR Substrate*

Sample substrate was fabricated using the protocol of a previously published report.[23] Cover slides (12 mm ∅) were cleaned in piranha solution (3:1 H_2SO_4/30%H_2O_2). After the piranha cleaning, the slides were thoroughly rinsed with DW three times and dried. To coat the cover slides with amino-group, the cover slides were then immersed in 5 mL of DW containing 100 μL of aminopropyltrimethoxysilane solution for 24 h. After the reaction, the cover slides were rinsed with excess of DW and ethanol and dried. Subsequently, the amino-group–coated cover slides were immersed in PGNR solution (0.473 mM) for 24 h, rinsed with DW, and dried. The sample substrate (the cover slides

covered with PGNRs) was then immersed into solution that contained dopamine-functionalized MT1-MMP–specific cleavable peptide (MSCP) solution for the immobilization of MSCP onto GNRs. Here, the dopamine-functionalized MSCP was prepared as follows: 1 mg of MSCP dissolved into 10 mL of phosphate-buffered saline (PBS) buffer (pH 7.4). Subsequently, 1 mL of dopamine solution (0.9 mg/mL) was added to the solution and stirred vigorously; 1-ethyl-3-(3-dimethylaminopropyl)-carbodiimide (1.1 mg) and sulfo-*N*-hydroxysulfosuccinimide (1.2 mg) were then added to the solution, and the reaction mixture was stirred for 4 h. The dopamine, one of the composing materials of dopamine-functionalized MSCP solution, is used as an anchoring agent on the surface of GNRs via robust Au–catechol interaction.[24] These dopamine molecules interact with the surface of gold via its functional unit, the catechol group. At the catechol group, the associated dipole moment and the reactivity of oxygen toward metals play a role in the metal–molecule interaction.

3.3 *Preparation of Enzyme-Dissolved Solutions and Cell Lysates*

To obtain MT1-MMP–dissolved solution, (100, 10, and 1 nM, respectively), the recombinant catalytic domain of human MT1-MMP, which is initially dissolved in stock solution with concentration of 0.2 mg/mL, was diluted in a PBS solution at room temperature. The whole-cell lysates (2×10^6 cells/mL) used radioimmunoprecipitation assay buffer composed of 50 mM Tris-HCl (pH 7.4), 150 mM NaCl, 1% Triton X-100, 1 mM ethylenediaminetetraacetic acid, 1 mM sodium orthovanadate, 1 mM phenylmethylsulfonyl fluoride, and proteinase inhibitors.

3.4 *Detection of LSPR Signal*

A sample chip was assembled composed of two separate cover slides, in which one slide was coated with PGNRs and the other slide was empty. The two glass slides were sealed with vacuum grease, and the sample chip was vertically mounted on our home-built LSPR system between a quartz-tungsten-halogen light source (Ocean Optics, Dunedin, Florida, HL2000) with focusing lens and a portable spectrometer (Ocean Optics, USB4000) with collimating lens.

4 Results and Discussion

4.1 *LSPR Substrate Preparation*

We prepared LSPR substrate for recognition of proteolytic activity about MT1-MMP anchored on invasive cancer cells (Fig. 1). GNRs were prepared using previously published protocols.[21] For the effective immobilization of GNRs onto glass substrate, we prepared PEG-coated GNRs (PGNRs). The end terminal groups of PEG were composed of carboxyl and thiol groups, respectively. The thiol group of PEG was conjugated with surface of GNRs and so the surface of GNRs was modified with PEG. After the preparation of PGNRs, absorbance spectrum was measured (Shimadzu, UV-1800) that dispersed in DW. As shown in Fig. 2(a), the absorbance peaks of PGNRs were exhibited at 780 and 520 nm. These absorbance peaks were generated because of collective oscillation of electrons surrounding PGNRs along the longitudinal and transverse axes of PGNRs, respectively. Subsequently, we immobilized PGNRs onto amine group–coated glass substrate, and adsorbed PGNRs were observed by dark field microscopy (BX51, Olympus, Japan) using a high numerical aperture dark field condenser (U-DCW, Olympus), which delivers a very narrow beam of white light from a tungsten halogen lamp to the surface of the sample. As can be seen from Fig. 2(b), the surface density of PGNRs was 411 #/μm^2 on the substrate, and the coated PGNRs on aminated glass substrate were observed as green color dot in the dark field microscopic image due to its optical properties,

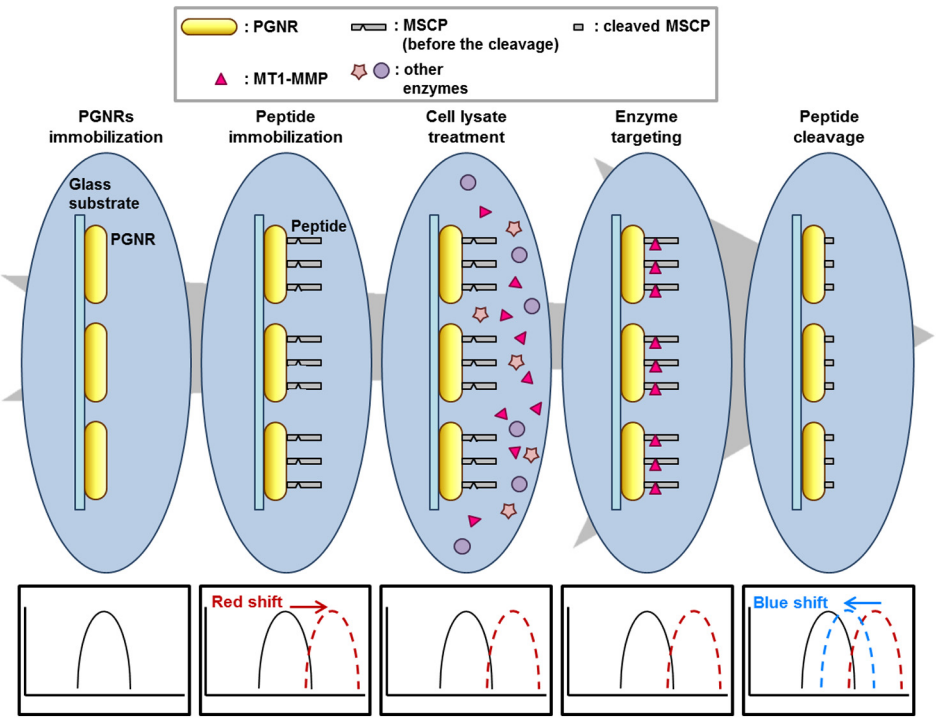

Fig. 1 Schematic illustration for process of localized surface plasmon resonance (LSPR) sensor preparation and LSPR spectra acquisition for detection of membrane type 1 matrix metalloproteinase (MT1-MMP).

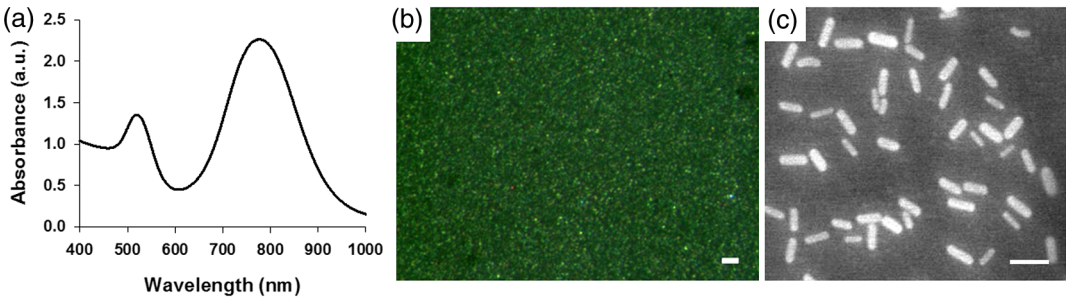

Fig. 2 (a) Absorbance spectrum of PGNR in water. (b) Dark field microscopic image and (c) transmission electron microscopy image of PGNR adsorbed on glass substrate. Scale bar is 2 μm in (b) and 50 nm in (c).

especially in absorbance property. In the absorbance spectrum of PGNRs, they have a peak at 520 nm in visible region, so PGNRs on glass substrate were strongly absorbed light corresponding to 520 nm. Because PGNRs absorbed light at 520 nm strongly, they scattered light that has almost the same wavelength. In addition, we also observed size and morphology of PGNRs adsorbed on glass substrate using scanning electron microscopy (JSM-7001F, JEOL Ltd.) [Fig. 2(c)]. We determined that the longitudinal length of PGNRs was 35.2 ± 1.5 nm and the transverse length of PGNRs was 10.8 ± 0.9 nm ($n = 100$). The aspect ratio (longitudinal length/transverse length) of PGNR is, therefore, about 3.5 using above mentioned values. The relationship between aspect ratio and peak wavelengths of PGNRs was in good agreement with previously published report.[18] Collectively, these results suggest that PGNRs are uniformly immobilized onto glass substrate, and the prepared sample substrate have potential for LSPR sensing substrate of proteolytic activity of MT1-MMP anchored on cancer cells.

4.2 *Sensitivity Measurement*

First of all, the local index sensitivity of bare PGNRs-coated substrate was investigated by measuring LSPR extinction spectra using various dielectric media that have different RIs, i.e., air: 1.000, water: 1.333, ethanol: 1.362, 1-propanol: 1.387, dimethylformamide: 1.428, and chloroform: 1.490 [Fig. 3(a)]. As RI of dielectric media was increased, the peak wavelength of LSPR extinction spectrum was red shifted. Subsequently, we also calculated sensitivity of LSPR substrate to changes in RI of surrounding dielectric media, and the sensitivity of LSPR substrate was yielded 169.8 nm/RI unit (RIU) [Fig. 3(b)]. This value was similar to other previously published reports using ensembles of GNRs.[25] In these results, we confirmed that prepared LSPR substrate is applicable to detect the low concentration of biomolecules as varying the surrounding RI of PGNRs. Subsequently, we also measured LSPR signals from MSCP-conjugated PGNRs in DW, and the red-shifted LSPR spectrum was shown in Fig. 3(c). The $\Delta\lambda_{max}$ red-shift of LSPR spectra was calculated as 31 nm compared with bare PGNRs in DW.

4.3 *Sensing for Proteolytic Activity of MT1-MMP*

Before the detection of proteolytic activity of MT1-MMP for cell lysates, we studied the capability of prepared LSPR substrate for detection of MT1-MMP enzymes using MSCP-conjugated PGNRs [Fig. 4(a)]. To investigate the specific interaction between MT1-MMP enzymes and MSCP-conjugated PGNRs, we performed experiments measuring the blue-shift of λ_{max} as varying the reaction time and MT1-MMP concentration. Based on the λ_{max} blue-shift of LSPR spectra due to proteolytic activity from MT1-MMP, we confirmed that the efficiency of

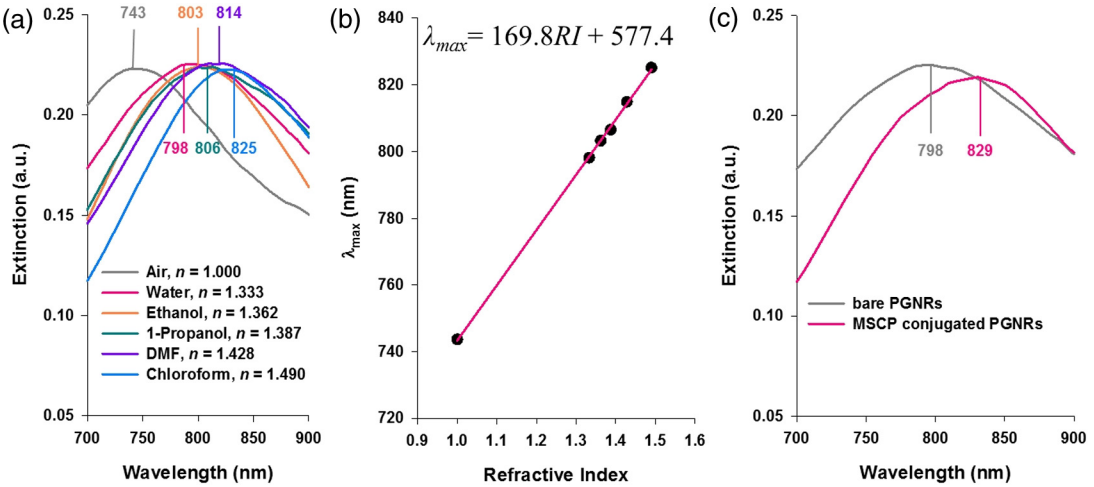

Fig. 3 (a) Spectra of PGNR absorbed on glass substrate in different dielectric media. (b) Sensitivity of LSPR chip according to refractive index of dielectric media environments. The slope of the fitted line represents the sensitivity of 169.8 nm/RIU. (c) Spectra of bare PGNRs and MT1-MMP specific cleavable peptide (MSCP)-conjugated PGNRs.

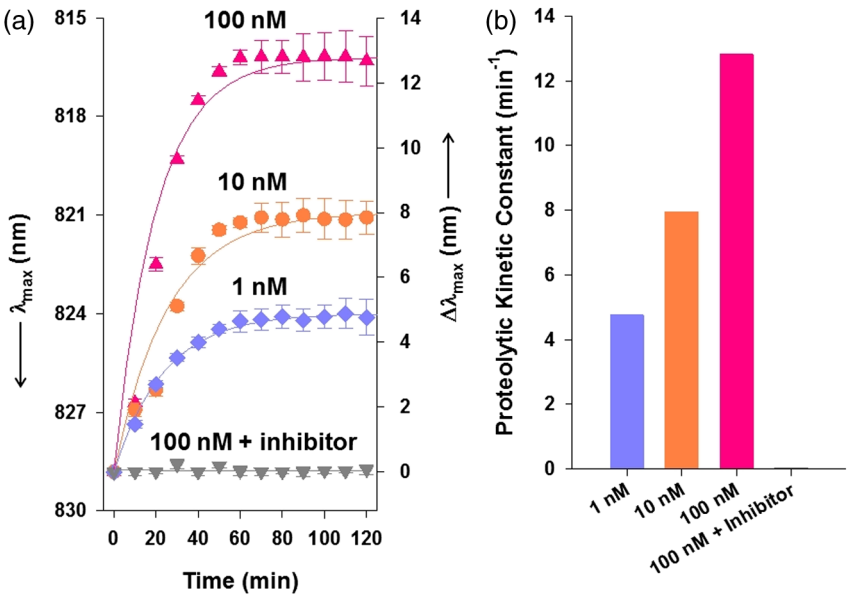

Fig. 4 (a) Maximum wavelength (λ_{max}) and shifts ($\Delta\lambda_{max}$) as a function of time owing to proteolysis in different concentration of MT1-MMP and treated with inhibitor (GM6001). (b) Proteolytic kinetic constant (k_p) with respect to MT1-MMP concentration and inhibitor existence.

proteolysis is dominantly determined by MT1-MMP concentration. As the concentration of MT1-MMP increased, λ_{max} blue-shift of LSPR spectra was also increased and, as a result, higher plateau value was exhibited. Moreover, we calculated the *in situ* proteolytic activity for each condition to obtain quantitative kinetic constant of proteolysis. For the understanding of kinetics of proteolytic activity determined by λ_{max} blue-shift of LSPR spectra, the Langmuir kinetic model was applied.[26,27] Langmuir kinetic model demonstrates the rate equation for dissociation of molecules on the sample surface. We hypothesized that enzymatic and proteolytic activity is an irreversible process, cleaved peptides cannot be specifically bound to remain peptides on PGNRs. The Langmuir kinetic model provides that $N(t) = N_0 \exp(-k_p t)$, where N_0 is the number of peptides immobilized on the surface of PGNRs at initial time. The number of cleaved peptides, thus, is given by $\Delta N_p(t) = N_0 [1 - \exp(-k_p t)]$. Using Langmuir kinetic model that describes as $\Delta N_p(t) = N_0 [1 - \exp(-k_p t)]$, we fitted graphs and extracted proteolytic kinetics constant (k_p) for each condition [Fig. 4(b)]. For the validation of specific activity for MT1-MMP, we also investigated λ_{max} blue-shift of LSPR spectra using MT1-MMP inhibitor, GM6001. Before the treatment of MT1-MMP, LSPR substrate was incubated with GM6001 (100 nM) to block the MT1-MMP–specific cleavage. Although the concentration of MT1-MMP was 100 nM, the cleavage of MSCP did not occur, so the λ_{max} blue-shift of LSPR spectra was also not exhibited. Accordingly, the proteolytic kinetic constant, therefore, was almost zero. These results indicate that our LSPR-based nanobiosensor shows a potential of sensitive detection for proteolytic activity for MT1-MMP.

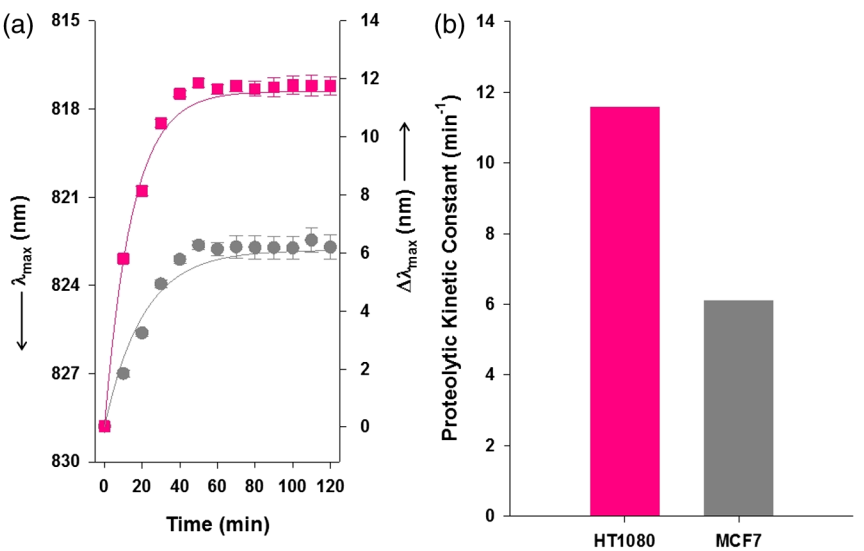

Fig. 5 (a) Maximum wavelength (λ_{max}) and shifts ($\Delta\lambda_{max}$) as a function of time owing to proteolysis of MT1-MMP from HT1080 and MCF7 cells. (b) Proteolytic kinetic constant with respect to cell lines (HT1080 and MCF7 cells).

4.4 *Sensing for Proteolytic Activity of Invasive Cancer Cells*

We preferentially conducted real-time polymerase chain reaction to investigate expression levels of MT1-MMP in HT1080 and MCF7 cells (data not shown). We selected a control gene, glyceraldehyde 3-phosphate dehydrogenase (GAPDH) gene, because the it is uniformly expressed within most cells and is hardly altered by drugs or other chemical agents. The relative expression levels of MT1-MMP, compared with GAPDH, on HT1080 cells were higher than on MCF7 cells, by about 20-fold. To evaluate the potential of our LSPR-based nanobiosensor for cancer diagnosis, we studied detection of proteolytic activity of MT1-MMP using whole cell lysate extracted from live cancer cells. We observed λ_{max} blue-shift of LSPR spectra owing to proteolysis of MSCP by MT1-MMP using whole cell lysate of two different cancer cell lines (HT1080 and MCF7 cells) [Fig. 5(a)]. We also fitted using Langmuir kinetic model and proteolytic kinetics constant (k_p) [Fig. 5(b)] in each cancer cell using values of k_p determined in Sec. 4.3. For HT1080 cells (MT1-MMP over-expressed), the k_p value exhibits 11.58 min^{-1}, whereas in the case of MCF7 cells (MT1-MMP deficient), the k_p value shows 6.10 min^{-1}, so the proteolytic activity of HT1080 cells is higher by about twice than that of MCF7 cells in our LSPR sensor.

5 Conclusion

In conclusion, we developed activatable peptide-immobilized LSPR sensor for detection of proteolytic activity of MT1-MMP from invasive cancer cells. First of all, we prepared LSPR substrate and measured its sensitivity while varying the surrounding dielectric media having different RIs. We also investigated the proteolytic activity of MT1-MMP with respect to MT1-MMP concentration. Finally, we studied proteolytic activity of MT1-MMP anchored at invasive cancer cells. We believe that our activatable peptide-immobilized LSPR sensor is applicable for diagnosis and prognosis of cancer.

Acknowledgments

This work was supported by the National Research Foundation of Korea (NRF) funded by the Ministry of Education, Science and Technology (2012R1A1A2006248 and 2012R1A2A1A01011328) and a grant from the National R&D Program for Cancer Control, Ministry for Health and Welfare, Republic of Korea (1220100).

References

1. Y. Hong et al., "Nanobiosensors based on localized surface plasmon resonance for biomarker detection," *J. Nanomater.* **2012**(1), 759830 (2012).
2. B. Sepúlveda et al., "LSPR-based nanobiosensors," *Nano Today* **4**(3), 244–251 (2009).
3. N. Vogel et al., "Reusable localized surface plasmon sensors based on ultrastable nanostructures," *Small* **6**(1), 104–109 (2010).
4. K. Kessenbrock, V. Plaks, and Z. Werb, "Matrix metalloproteinases: regulators of the tumor microenvironment," *Cell* **141**(1), 52–67 (2010).
5. A. Page-McCaw, A. J. Ewald, and Z. Werb, "Matrix metalloproteinases and the regulation of tissue remodelling," *Nat. Rev. Mol. Cell. Biol.* **8**(3), 221–233 (2007).
6. M. Seiki, "Membrane-type 1 matrix metalloproteinase: a key enzyme for tumor invasion," *Cancer Lett.* **194**(1), 1–11 (2003).
7. T.-H. Chun et al., "MT1-MMP–dependent neovessel formation within the confines of the three-dimensional extracellular matrix," *J. Cell Biol.* **167**(4), 757–767 (2004).
8. E. I. Deryugina et al., "Unexpected effect of matrix metalloproteinase down-regulation on vascular intravasation and metastasis of human fibrosarcoma cells selected in vivo for high rates of dissemination," *Cancer Res.* **65**(23), 10959–10969 (2005).
9. Y. Zhai et al., "Expression of membrane type 1 matrix metalloproteinase is associated with cervical carcinoma progression and invasion," *Cancer Res.* **65**(15), 6543–6550 (2005).
10. M. Ouyang et al., "Visualization of polarized membrane type 1 matrix metalloproteinase activity in live cells by fluorescence resonance energy transfer imaging," *J. Biol. Chem.* **283**(25), 17740–17748 (2008).
11. T. Huang et al., "Photostable single-molecule nanoparticle optical biosensors for real-time sensing of single cytokine molecules and their binding reactions," *J. Am. Chem. Soc.* **130**(50), 17095–17105 (2008).
12. S. Chen et al., "Ultrahigh sensitivity made simple: nanoplasmonic label-free biosensing with an extremely low limit-of-detection for bacterial and cancer diagnostics," *Nanotechnology* **20**(43), 434015 (2009).
13. W. Zhou et al., "A label-free biosensor based on silver nanoparticles array for clinical detection of serum p53 in head and neck squamous cell carcinoma," *Int. J. Nanomed.* **6**(1), 381–386 (2011).
14. W. S. Hwang and S. J. Sim, "A strategy for the ultrasensitive detection of cancer biomarkers based on the LSPR response of a single AuNP," *J. Nanosci. Nanotech.* **11**(7), 5651–5656 (2011).
15. S. Chen et al., "Plasmon-enhanced colorimetric ELISA with single molecule sensitivity," *Nano Lett.* **11**(4), 1826–1830 (2011).
16. R. Gans, "Über die Form ultramikroskopischer Goldteilchen," *Annalen der Physik* **342**(5), 881–900 (1912).
17. R. Gans, "Über die Form ultramikroskopischer Silberteilchen," *Annalen der Physik* **352**(10), 270–284 (1915).
18. S. Link, M. B. Mohamed, and M. A. El-Sayed, "Simulation of the optical absorption spectra of gold nanorods as a function of their aspect ratio and the effect of the medium dielectric constant," *J. Phys. Chem. B* **103**(16), 3073–3077 (1999).
19. S. Eustis and M. A. El-Sayed, "Determination of the aspect ratio statistical distribution of gold nanorods in solution from a theoretical fit of the observed inhomogeneously broadened longitudinal plasmon resonance absorption spectrum," *J. Appl. Phys.* **100**(4), 044324–044327 (2006).
20. T. R. Jensen et al., "Nanosphere lithography: effect of the external dielectric medium on the surface plasmon resonance spectrum of a periodic array of silver nanoparticles," *J. Phys. Chem. B* **103**(45), 9846–9853 (1999).
21. Y. Hong et al., "Gold nanorod-mediated photothermal modulation for localized ablation of cancer cells," *J. Nanomater.* **2012**(1), 825060 (2012).
22. L. Eugene et al., "Highly selective CD44-specific gold nanorods for photothermal ablation of tumorigenic subpopulations generated in MCF7 mammospheres," *Nanotechnology* **23**(46), 465101 (2012).
23. J. Yang et al., "In situ detection of live cancer cells by using bioprobes based on Au nanoparticles," *Langmuir* **24**(21), 12112–12115 (2008).
24. H. Lee et al., "Fluorescent gold nanoprobe sensitive to intracellular reactive oxygen species," *Adv. Func. Mater.* **19**(12), 1884–1890 (2009).
25. K. M. Mayer et al., "A label-free immunoassay based upon localized surface plasmon resonance of gold nanorods," *ACS Nano* **2**(4), 687–692 (2008).
26. T. Kwon et al., "Nanomechanical in situ monitoring of proteolysis of peptide by cathepsin B," *PLoS One* **4**(7), e6248 (2009).
27. G. Lee et al., "Real-time quantitative monitoring of specific peptide cleavage by a proteinase for cancer diagnosis," *Angew. Chem. Int. Ed.* **51**(24), 5837–5841 (2012).